A comparative study on the hydro-mechanical behaviour of compacted bentonite/sand plug based on laboratory and field infiltration tests

Qiong Wang, Anh Minh A.M. Tang, Yu-Jun Cui, Jean-Dominique Barnichon, Wei-Min Ye

1 # A comparative study on the hydro-mechanical behaviour of

2 ## compacted bentonite/sand plug based on laboratory and field

3 ## infiltration tests

4 Qiong Wang[1], Anh Minh Tang[1], Yu-Jun Cui[1,3],

5 Jean-Dominique Barnichon[2], Wei-Min Ye[3]

6

7 *[1] Ecole des Ponts ParisTech, France*
8 *[2] Institut de Radioprotection et de Sûreté Nucléaire (IRSN), France*
9 *[3] Tongji University, China*

10

11

12

13

14

15

16 <u>**Corresponding author:**</u>
17 Prof. Yu-Jun CUI
18 *Ecole des Ponts ParisTech*
19 6-8 av. Blaise Pascal, Cité Descartes, Champs-sur-Marne
20 77455 MARNE LA VALLEE
21 France
22
23 Telephone: +33 1 64 15 35 50
24 Fax: +33 1 64 15 35 62
25 E-mail: yujun.cui@enpc.fr

26

Abstract: SEALEX is a research project aiming at identifying the key factors that affect the long-term performance of bentonite-based sealing systems with an initial technological void. In this context, a series of in-situ experiments have been being performed in field conditions. Meanwhile, a small scale test (1/10) was carried out in controlled conditions in the laboratory, aiming at providing useful information for analyzing the in-situ tests in terms of saturation time and sealing effectiveness. In this paper, the results of the small-scale test are presented along with the results from the first in-situ test (PT-N1). It was observed that during the saturation process, the evolution of the injected water volume followed a hyperbolic relationship with time in both the laboratory and field conditions. In the laboratory conditions, a decrease in axial swelling pressure occurred due to filling of the technological void. By contrast, this decrease has not been observed in the field conditions. Comparison of the injected water and the axial swelling pressure between the two different scales enabled the definition of a same time up-scaling ratio of 2.5 (in situ experiment /small scale test). Accordingly, the saturation duration of the in situ experiment was estimated to be equal to two years. For the small-scale test, a swelling strain evolution rate of 0.588 mm/day was identified in the case of infiltration from two sides of the sample. This is useful when predicting the evolution of swelling strain in the case of failure of the sealing plug. After filling of an additional 20% void, a swelling pressure of 0.18 MPa was obtained, indicating the favorable sealing capacity of the material after filling the technological void.

49   void; swelling pressure; swelling stain.

1 INTRODUCTION

51   In the design of deep geological repository for high level long lived radioactive wastes,

52   compacted bentonite-based materials are often considered as buffer/sealing materials.

53   These materials are expected to exhibit a swelling pressure high enough to fulfil their

54   buffer/sealing functions.

55   Numerous laboratory studies have been conducted to assess the performance of

56   buffer/sealing materials (e.g. Delage et al., 1998; Lloret et al., 2003; Romero et al.,

57   2005; Lloret & Villar, 2007). Various experiments were also performed in the

58   underground research laboratories (URL) (TSX at Manitoba, Canada; FEBEX at

59   Grimsel, Switzerland; RESEAL at Mol, Belgium; KEY at Bure, France, etc.).

60   Recently, IRSN (Institut de Radioprotection et de Sûreté Nucléaire, France) has

61   launched the SEALEX project aiming at identifying and quantifying the key factors

62   related to the long-term performance of bentonite-based sealing systems taking into

63   account an initial technological void. This project consists of a series of in-situ

64   experiments in the Tournemire URL, and a small-scale test (1/10) in the laboratory.

65   The in-situ experimental program was purposefully built allowing systematical

66   exploration of the effects of technical specifications, design, construction, defect, etc.,

67   by changing a single parameter each time. As a reference case (see Barnichon et al.

68   2009, 2012 for more details), the first test PT-N1 with a clay core made up of

69   pre-compacted monolithic disks of MX80 bentonite/sand mixture (70/30 in dry mass)

70   has been conducted in the URL of Tournemire. Due to the low permeability of this

71   material, saturation is expected to be reached in several years (see Barnichon et al.,

72   2012). During the saturation process, the injected water volume, total pressure, pore

73   water pressure and relative humidity changes have been monitored at several

74   positions within the plug. After the saturation stage, hydraulic tests will be performed

75   to determine the overall hydraulic properties (permeability, occurrence of leakage) of

76   the sealing system. In addition to this reference case, three other tests are designed to

77   quantify the impact of the technical specification and design of the sealing plug by

78   changing the intra-core geometry (jointed in stead of monolithic disks), core

79   composition (MX80/sand ratio) and core conditions (compacted in field in stead of

80   pre-compacted). Moreover, to investigate the effect of altered conditions, an

81   additional test is designed to simulate an incidental decrease of swelling pressure

82   caused by failure of the confining structure.

83   Based on the design of the in-situ experiments, a laboratory small-scale test (1/10)

84   was performed, focusing on the recovery capacity of the bentonite-based seal with

85   technological voids. The material identical to that used in test PT-N1 was used (MX80

86   bentonite/sand mixture). A confining cell of stainless steel was used to simulate the

87   constant-volume boundary conditions. After the initial saturation process as in the

88   PT-N1 in-situ experiment, the seal evolution upon a confinement failure was

89   simulated by allowing a given amount of free swell. This free swell was followed by a

90   last stage of wetting under constant volume conditions. To assess the sealing capacity,

91   the injected water volume, axial swelling pressure and swelling strain were monitored

92 in different stages. It was expected to obtain useful information from the laboratory

93 small-scale test for analysing the field tests in terms of saturation time and sealing

94 effectiveness.

95 In this paper, the results of the small scale test are presented along with the results

96 from the in-situ test (PT-N1). An up-scaling ratio was obtained by comparing the

97 injected water volume and the axial swelling pressure evolution between the

98 laboratory and field conditions. The time needed to reach the stabilization of axial

99 swelling pressure for the in situ test (PT-N1) as well as the evolution of swelling strain

100 and swelling pressure in the case of failure of the confining structure were estimated

101 accordingly.

2 MATERIALS AND METHODS

2.1 Materials

The soil studied is a compacted MX80/sand mixture with a proportion of 70/30 in dry

mass. The bentonite is from Wyoming, USA, with a high content of montmorillonite

(80%). It has a liquid limit of 575%, a plastic limit of 53% and a unit mass of

2.77 Mg/m^3. The cation exchange capacity (CEC) is 76 meq/100g (83 % of Na^+). The

quartz sand used in the mixture comes from Eure and Loire (France) with a unit mass

of 2.65 Mg/m^3. It was sieved at 2 mm prior to being mixed with the bentonite.

The water used has the same chemical composition as the pore water of the

Callovo-oxfordian claystone from the ANDRA URL in Bure (France), namely

synthetic water (Wang et al., 2012a, 2012b). It was obtained by mixing the

113   corresponding chemical compounds (see Table 1) with distilled water using a

114   magnetic stirrer until full dissolution.

115   **2.2 SEALEX in-situ test (PT-N1)**

116   As mentioned above, the in-situ experiment (PT-N1) has been conducted in the

117   Tournemire Underground Research Laboratory excavated in Toarcian claystone. A

118   horizontal borehole (0.60 m in diameter) was drilled for this purpose. Figure 1 shows

119   the layout of the experiment. A seal made up of compacted MX80/sand mixture was

120   sandwiched between two porous plates, allowing water inflow from two water

121   reservoirs (i.e. upstream and downstream). The 14.33% annular technological void

122   (volume of void/volume of borehole) was defined by adopting a smaller initial

123   diameter (0.555 m) of the pre-compacted seal as compared to the borehole diameter

124   (0.60 m). The upstream plate is in direct contact with the host-rock while the

125   downstream one is retained by a confining system ensuring a constant-volume

126   condition. A packer-like device was used to prevent water leakage from the interface

127   between the confining plug and host-rock.

128   The clay seal in test PT-N1 is made up of 8 monolithic pre-compacted disks (0.555 m

129   in diameter and 0.15 m thick) of MX80/sand mixture with an initial dry density of

130   1.97 Mg/m^3 (Figure 2). The disks were arranged in vertical slices giving rise to the

131   geometry of seal as shown in Figure 2. The bricks were obtained through uniaxial

132   compaction of the mixture at its initial water content of 11%. The initial dry density

133   (1.97 Mg/m^3) of the bricks was selected based on the consideration of the 14.33 %

134   technological void and the need to have a final dry density of 1.67 Mg/m^3 after

135   saturation of the plug and filling of the initial technological voids.

136   Three types of sensors were installed within the compacted blocks to monitor the

137   swelling pressure, pore pressure and relative humidity. For clarity, only the

138   distribution of sensors for swelling pressure measurement is shown in this paper

139   (Figure 3a). Three total pressure sensors were installed on the surface of the column at

140   section 0.60 m (from the downstream saturation system, L-01, L-02, L-03) to measure

141   the radial swelling pressure; two total pressure sensors were installed at section 0 and

142   1.20 m to measure the axial swelling pressure (A-01, A-02). For each sensor, a hole as

143   shown in Figure 3b was prepared at their pre-assigned positions before the

144   assemblage of blocks, keeping the hole to a minimum size. Wireless sensors (d = 32

145   mm) were used to limit preferential flow along cables and a wireless transmitter was

146   installed at each measurement section. Data were recorded automatically by a data

147   acquisition system.

148   Regarding the test operational phases, a volume of water of 49 L was first injected,

149   which corresponded to the volume of the technological void adopted. This process

150   ended in one hour. Afterwards, the water supply was stopped because the side packer

151   was not properly inflated; it restarted after 20 days under a water pressure of 0.1 MPa.

152   During the saturation process, the swelling pressure, pore pressure, water content or

153   water saturation within the plug were monitored. The injected water volumes at both

154   upstream and downstream chambers were also measured. When the saturation process

155   is completed, hydraulic tests will be performed to determine the overall hydraulic

156   properties (permeability, occurrence of leakage) of the corresponding sealing systems.

2.3 Laboratory small-scale test

The experimental devices used for the laboratory small-scale test (1/10) are shown in Figure 4. A stainless steel cell of 60 mm in inner diameter and 200 mm long was used. As in the in-situ test, an annular technological void was defined by adopting a smaller initial diameter (55.5 mm) for the pre-compacted sample as compared to the diameter of the hydration cell (60 mm). Note however that the hydration cell was placed in the vertical direction (see Figure 4) and it was then different from the in-situ test which is performed in a horizontal borehole (see Figure 1 and Figure 2). Water supply was conducted through the water inlets in the bottom base which was connected to burettes. This allowed measurement of the total amount of water taken up by the sample. A piston of 60 mm diameter was used to simulate the confining structure. On the bottom of the piston, there was drainage with two inlets (upside inlet in Figure 4) and a porous stone of 50 mm diameter, allowing water/air flow. A mechanical press was used to restrain the axial deformation and a force transducer was used to monitor the axial swelling pressure. A displacement transducer fixed on the piston allowed monitoring of the axial displacement to an accuracy of 1 μm. The axial pressure and axial displacement were recorded automatically to a data logger, while the inlet water volume was measured manually by determining the water level in the burettes. Note that in this small-scale test, the radial swelling pressure was not measured.

A monolithic cylindrical sample (55.5 mm in diameter, 120 mm high) was used in the test. It was statically compacted in a mould to the same dry density as in the in-situ test (1.97 Mg/m^3). In order to ensure the homogeneity of the specimen, the

8

179 compaction was carried out in two layers. The surface of the first compacted layer

180 was carefully scarified before the second layer was added to ensure a good junction

181 between them. Figure 5a shows the pre-compacted specimen with the hydration cell.

182 After compaction, the specimen (55.5 mm in diameter) was placed at the center of the

183 cell (60 mm in inner diameter), leaving an annular void (2.25 mm) between the

184 specimen and cell wall (Figure 5b). An initial axial stress of 0.1 MPa was applied on

185 the specimen before hydration in order to ensure good contacts between the load cell

186 and the piston, between the piston and the sample, between the sample and the cell

187 bottom, as well as satisfactory load measurement. Then, the upside inlets (see Figure

188 4) were sealed and vacuum was applied to evacuate all air in the voids (technological

189 void mainly). The synthetic water was finally injected from the bottom.

190 As described in Figure 6, hydration was carried out in three stages. First, the axial

191 deformation was restrained and water was injected to the sample; during this stage

192 (Stage 1. initial saturation phase), the evolution of the vertical swelling pressure was

193 monitored. Once the hydration ended, the confining pressure in the axial direction was

194 removed by unloading, allowing a free swell of 20% (Stage 2. recovery of the void

195 phase). To reduce the test duration in this stage, two-side infiltration was applied by

196 injecting water from both the bottom and the top, while recording changes in axial

197 swelling strain over time. This stage aimed at simulating the case of a saturation

198 defect or a failure of confining structure that may occur during the long-term lifespan

199 of the disposal system. The free swell of 20% represents the sealing capacity required

200 after filling the technological void. When the axial swelling strain reached the desired

201 value of 20%, the piston was automatically blocked thanks to a reserved distance of

202 24 mm (corresponding to 20% swelling strain) between the piston and the load cell

203 (Figure 7); the evolution of swelling pressure was monitored again (Stage 3.

204 confinement phase).

3 EXPERIMENTAL RESULTS

3.1 In situ test (PT-N1)

207 Figure 8 shows the evolution of injected water volume over time. As mentioned above,

208 a volume of 49 L was first injected to fill the technological void and the injection was

209 stopped for 20 days due to a technical problem related to the packer. After resuming

210 the injection, it was observed that the increase rate of water volume was followed by

211 an asymptotic curve with a decreasing rate. After 367 days, the total injected water

212 volume was 71.39 L (Figure 8). Examination of the curve shows that the shape of

213 water volume versus time (after rejection) can be described by a hyperbolic function.

214 Figure 9 presents the time/water volume (day/L) versus time. A good linear

215 relationship is obtained, confirming that the water volume-time curve is of a

216 hyperbolic shape. Thereby, the following equation can be adopted for this

217 relationship:

$$\frac{t}{V} = a + bt \qquad \qquad \text{Eq.1}$$

219 where t is time, V is injected water volume, a and b are the intercept and the slope of

220 the straight line, respectively (Figure 9).

221 According to this hyperbolic relationship, the maximum water volume corresponds to

222 *1/b* (Eq.2), equal to 72.46 L. This is to be compared with the total volume of voids

223 including the technological void and the soil porosity: 69.1 L.

224
$$V_{ma\,x} = \lim_{t\to\infty}V(t) = \lim_{t\to\infty}\left(\frac{1}{a/t+b}\right) = \frac{1}{b}$$
Eq.2

225 During hydration, both the axial and radial swelling pressures were recorded by the

226 total pressure sensors (see Figure 3) and the results are shown in Figure 10. The data

227 by the sensor located at 1.20 m section for the axial swelling pressure measurement

228 were unfortunately not available; only the axial swelling pressure values at 0 m

229 section are presented. This pressure increased at an almost constant rate and reached

230 1.63 MPa after 367 days. For the radial swelling pressure, the evolution rates were

231 very different for the three sensors (see Figure 3); the pressure values reached were

232 1.78 MPa, 0.56 MPa and 1.05 MPa for sensors L-01, L-02 and L-03, respectively.

233 This indicates the heterogeneous radial swelling under the in-situ conditions.

234 **3.2 Small-scale test**

235 Figure 11 shows the measured water inflow over time. Once the water supply was

236 connected to the bottom inlet, water volume increased rapidly and reached 49 mL in a

237 few minutes. This value corresponded exactly to the volume of technological void

238 (49 mL). Afterwards, water volume increased gradually to reach a maximum value of

239 70.6 mL. No more water could infiltrate after about 200 days. The total volume of

240 void (including the technological void V_{tech} and the void inside the soil V_{v-s}) that

241 could be filled with water was estimated at 69.1 mL. The result shows that a little

242 more water was injected with respect to the estimated one (70.6 mL against 69.1 mL),

243   but the difference is quite small.

244   For further analyzing the evolution of water volume, the time/water volume (day/mL)

245   is plotted versus time in Figure 12. As in the case of in-situ test, a straight line is

246   obtained justifying a hyperbolic relationship between the water volume and the

247   elapsed time (Eq.1). The value of 1/b corresponds to the maximum volume of water:

248    $1/b = 71.43$ mL, which is very close to the measured water volume (70.6 mL).

249   Figure 13 and Figure 14 depict the evolution of swelling pressure in the first stage (i.e.

250   initial saturation phase). Once water was injected into the specimen, the axial swelling

251   pressure increased very quickly (Figure 14). After about 2 days, the swelling pressure

252   reached a first stability stage (1.30 MPa) and it restarted to increase on the 4th day.

253   When the swelling pressure reached 1.45 MPa after about 12 days, a significant

254   decrease of swelling pressure occurred and a minimum value of 0.70 MPa was

255   reached. Afterwards, the swelling pressure increased again after about 33 days (Figure

256   13), but at a slower rate. In addition, the evolution curve shows fluctuating pattern.

257   The swelling pressure reached a mean value of 1.80 MPa after 300 days and then

258   fluctuated in the range of 1.75-1.95 MPa.

259   The axial deformation during the swelling pressure development was also recorded,

260   and shown in Figure 13. It followed the same trend as the swelling pressure. Note

261   however that the variation of displacement was smaller than 0.2 mm. It represents

262   0.16% of the specimen height (120 mm), suggesting a satisfactory control of axial

263   displacement in this stage.

264 According to the data obtained in the first stage (Figure 13), no obvious swelling

265 pressure increase occurred during a period of 50 days from day 300 to day 350. Thus,

266 it was decided to start the second stage. For this purpose, the confining pressure was

267 removed on day 350, allowing the free swell. Changes in axial swelling strain were

268 recorded and presented in Figure 15. The uplifting of load cell led to an instantaneous

269 rebound of 1.1% (1.4 mm / 120 mm). Afterwards, the axial swelling strain increased

270 almost linearly at a rate of 0.145 mm/day. Following this rate, 20% of swelling strain

271 was expected to be reached after 157 days. In order to reduce the test duration, two

272 sides infiltration was applied on day 364. This resulted in an increase of the swelling

273 strain rate to 0.588 mm/day, which is four times faster than that with one-side

274 infiltration. The expected value of 20% (24 mm) was reached on day 400. The piston

275 was then re-blocked automatically to start Stage 3. Note that the measured axial swell

276 was 24.4 mm.

277 The evolution of swelling pressure was then measured again and the results are

278 presented in Figure 16. Small fluctuation was observed and this fluctuation can be

279 attributed to the daily temperature variations. As expected, the evolution curve follows

280 a hyperbolic curve with a decreasing rate over time. It reached stabilization on day

281 520 with a final swelling pressure of 0.18 MPa.

282 **4 COMPARISON AND DISCUSSION**

283 It was observed that more water infiltrated into the soil than that calculated by

284 considering the technological void and the soil porosity in both the in situ test

285 (71.39 L) and laboratory small-scale test (70.60 mL). Even though the water volume

286 has been not yet reached stabilization in the in-situ conditions, the discrepancy is

287 found to be larger than in the small-scale test. This can be related to the natural

288 conditions of the in-situ test, where some water intake by the host-rock did occur.

289 With a well controlled condition in the small-scale test, the larger infiltrated water

290 obtained may be related to the low water density (1.00 Mg/m^3) considered in the

291 determination of soil void ratio. Indeed, for high plasticity materials as the MX80

292 bentonite, the water density can be much higher than 1.00 Mg/m^3 (Marcial 2003,

293 Villar and Lloret 2004, Lloret and Villar 2007, Jacinto et al. 2012). This is in

294 agreement with the observation from the KBS-3H mock-up test (Börgesson et al.

295 2005).

296 Regarding the evolution of water volume, a hyperbolic relationship between the

297 injected water volume and elapsed time was obtained in both tests. Accordingly, the

298 maximum water volume was estimated at 72.46 L and 71.43 mL for the in-situ and

299 small-scale tests, respectively. To compare the evolution curve at different scales, the

300 water volume was normalized by using these two values. The normalized water

301 volume is equal to the ratio of water volume at time t (V_t) to the maximum water

302 volume that can be injected (72.46 L and 71.43 mL for the in-situ and small-scale test,

303 respectively). In terms of time scale, an up-scaling ratio of 2.5 (in situ test/small scale

304 test) was found from the normalized water volume shown in Figure 17, where very

305 similar evolution curves (normalized water volume versus normalized time) were

306 obtained for the two tests (in situ and small scale tests).

307   This up-scaling ratio is much smaller than that estimated based on the consolidation

308   theory by considering the experiment scale and hydration conditions: according to the

309   infiltration length, the hydration rate of the in-situ test should be 100 times lower than

310   in the small-scale test (1/10). As the two-side infiltration applied in the in-situ test

311   increased the hydration rate by 4 times, the up-scaling ratio should be equal to 25

312   (in-situ test / small scale test), still ten time larger than the rate identified from the

313   measurements. In fact, under the field conditions, water may fill some voids between

314   the pre-compacted disks during the first minutes (0.15 m thick, see Figure 2). This

315   infiltration length of 0.15 m leads to an up-scaling ratio to 0.56. The up-scaling ratio

316   of 2.5 observed is possibly related to the combined effect of these two phenomena.

317   Using this up-scaling ratio, the axial swelling pressure evolution curve obtained from

318   the in-situ test (Figure 10) was normalized and presented in Figure 18, together with

319   the axial swelling pressure measured in the first stage of the small-scale test. Except

320   for the first 33 days (see Figure 13) where significant decrease of swelling pressure

321   occurred in the small-scale test, the normalized curve of swelling pressure for the

322   in-situ test join the curve of the small-scale test, confirming the up-scaling ratio of 2.5.

323   Based on the results of small-scale test, this ratio allows the time needed to reach the

324   stabilization of swelling pressure in the in-situ test to be estimated. It can be observed

325   in the small-scale test that the swelling pressure reached the stability after about 300

326   days. Thus, 155 days more is needed to reach the maximum swelling pressure at the

327   normalized time scale for the in-situ test. Accordingly, it can be estimated that the

328   maximum swelling pressure in the in-situ test should be reached after 388 days,

329   corresponding to 754 days starting from the time of water injection.

330   As regards the kinetics of the axial swelling pressure in the first 33 days of small-scale

331   test, stabilization was attained after about 2 days at 1.30 MPa and restarted to increase

332   from day 4 (Figure 14). Wang et al. (2012b) observed similar phenomenon in swelling

333   pressure tests on smaller samples (35 mm in diameter, 10 mm in height) with the same

334   percentage of technological void. This is related to changes in microstructure of soil.

335   With the progress of hydration, the effect of microstructure changes is reduced,

336   resulting in the re-increase in swelling pressure (Cho et al., 2000; Baille et al., 2010).

337   When the swelling pressure reached 1.45 MPa on day 12, a significant decrease of

338   swelling pressure occurred, reaching a minimum value of 0.70 MPa. This decrease

339   can be attributed to the filling of the technological void. Afterwards, the swelling

340   pressure increased again from day 33. However, the evolution curve showed

341   fluctuation due to the re-organization of soil microstructure under the effect of

342   technological void.

343   On the contrary, the axial swelling pressure measured in the in-situ test increased

344   constantly without any fluctuation. This can be related to a coupled effect of large

345   scale and pressure sensor location. Indeed, in the small-scale test, the axial swelling

346   pressure was measured on the whole cross section and any changes in axial pressure

347   could be monitored. However, in the in situ test, the total pressure sensor was installed

348   in the centre of the cross section (Figure 3) and the axial swelling pressure herein

349   corresponded to the local one. Therefore, the axial swelling pressure changes occurred

350   in the zone of technological void could not be detected by this sensor.

351   After the axial swelling pressure of small-scale test reached stabilization, removing

352   the axial confining restriction led to a very small rebound of 1.1% (1.4 mm/ 120 mm).

353   This observation provides valuable information for the confinement removal phase of

354   the in-situ test. During the free swelling process (Stage 2), a swelling strain evolution

355   rate (swelling strain/time) of 0.588 mm/day was observed under two-side infiltration

356   conditions. Combined with the up-scaling ratio, this result (0.588 mm/day) allows

357   prediction of the swelling strain evolution in the in-situ test when simulating an

358   incidental decrease of the swelling pressure caused by a failure of the concrete

359   confining structure.

360   As the piston was re-blocked automatically in the small-scale test (Stage 3), swelling

361   pressure developed again. This indicates the favorable sealing capacity after filling of

362   the technological void. If a saturation defect or a confining structure failure occurs in

363   the field, a 20% additional void could be sealed. A final swelling pressure of

364   0.18 MPa was attained, which is in accordance with the swelling pressures measured

365   in the laboratory on smaller samples (Wang et al., 2012b): after the 20% free swell

366   (24.5 mm), the dry density decreased to a final value of 1.39 Mg/m^3; this corresponds

367   to a swelling pressure of 0.23 MPa.

368   **5 CONCLUSION**

369   In the context of SEALEX project, a laboratory small-scale test (1/10) was carried out

370   to investigate the recovery capacity of bentonite-based plug with technological void.

371   By comparison with the first results from the in-situ test PT-N1, the phenomena

372   identified in the laboratory were used for interpreting and estimating the results from

373   the in-situ test.

374   During the saturation process, a hyperbolic relationship between the injected water

375   volume and elapsed time was obtained in both laboratory and field tests. However, a

376   little more water was injected as compared to the water volume estimated by

377   considering the total porosity. Larger discrepancy was found for the in-situ test due to

378   the effect of natural conditions.

379   Decrease of axial swelling pressure was observed in the small-scale test due to the

380   filling of technological void. In contrast, the axial swelling pressure measured

381   increased continually in the in-situ test. This could be attributed to the effects of both

382   the scale and the locations of pressure sensors.

383   Comparison of the injected water volume and the axial swelling pressure between the

384   two different scales gave the same up-scaling ratio of 2.5 (in-situ scale / laboratory

385   scale). Using this up-scaling ratio, the time needed to reach the swelling pressure

386   stabilization in the in-situ test was estimated at 754 days.

387   After removal of the axial confining restriction, a swelling strain evolution rate

388   (swelling strain/time) of 0.588 mm/day was observed in the case of two-side

389   infiltration. Combined with the up-scaling ratio, this rate allowed prediction of the

390   swelling strain evolution in case of a confining structure failure. A swelling pressure

391   of 0.18 MPa was obtained after filling an additional void of 20%, indicating the

392   favorable sealing capacity after filling the technological void.

398 **REFERENCES**

399 Baille, W., Tripathy, S. & Schanz, T. 2010. Swelling pressures and one-dimensional
400   compressibility behaviour of bentonite at large pressures. Applied Clay Science, Vol 48,
401   324-333

402 Barnichon, J.D. & Deleruyelle, F. 2009. Sealing Experiments at the Tournemire URL.
403   EUROSAFE.

404 Barnichon, J.D., Dick, P. & Bauer, C. 2012. The SEALEX in situ experiments: performance
405   test of repository seals. Harmonising Rock Engineering and the Environment – Qian &
406   Zhou (eds) Taylor & Francis Group, London. ISBN 978-0-415-80444-8, pages
407   1391-1394.

408 Börgesson, L., Sandén, T., Fälth, B., Åkesson, M. & Lindgren, E. 2005. Studies of Buffers
409   Behaviour in KBS-3H Concept: Work During 2002-2004, SKB, R-05-50.

410 Cho, W.J., Lee, J.O., & Kang, C.H. 2000. Influence of temperature elevation on the sealing
411   performance of a potential buffer material for a high-level radioactive waste repository.
412   Annals of Nuclear Energy, Vol 27, 1271-1284

413 Delage, P., Howat, M.D. & Cui., Y.J. 1998. The relationship between suction and swelling
414   properties in a heavily compacted unsaturated clay. Engineering Geology, 50(1-2),
415   31-48.

416 Jacinto, A.C., Villar, M.V. & Ledesma, A. 2012. Influence of water density on the
417   water-retention curve of expansive clays, Ge´otechnique 62, No. 8, 657–667

418 Lloret, A., Villar, M.V., Sánchez, M., Gens, A., Pintado, X. & Alonso, E.E. 2003. Mechanical
419   behaviour of heavily compacted bentonite under high suction changes. Ge´otechnique 53,
420   No. 1, 27–40

421 Lloret, A. & Villar, M. 2007. Advances on the knowledge of the thermo-hydro-mechanical
422   behaviour of heavily compacted FEBEX bentonite. Physics and Chemistry of the Earth,
423   32, 701-715

424 Marcial, D. 2003. Comportement hydromécanique et microstructural des matériaux de
425   barrière ouvragée, PHD thesis, École Nationale des Ponts et Chaussées, Paris, France.

426 Romero, E., Villar, M. V. & Lloret, A. 2005. Thermo-hydro-mechanical behaviour of heavily
427   overconsolidated clays. Engng Geol. 81(3): 255 – 268.

428 Villar, M.V. & Lloret, A. 2004. Influence of temperature on the hydro-mechanical behaviour
429   of a compacted bentonite. Applied Clay Science, 26(1-4), 337-350.

430 Wang, Q., Tang, A. M., Cui, Y.J., Delage, P. & Gatmiri, B. 2012a. Experimental study on the

431   swelling behaviour of bentonite/claystone mixture, Engineering Geology, Vol. 124,
432   59–66.
433 Wang, Q., Tang, A. M., Cui, Y.J., Delage, P., Barnichon, J.D. & Ye, W.M. 2012b. The effects
434   of technological voids on the hydro-mechanical behaviour of compacted bentonite-sand
435   mixture. Soils and Foundations, Vol. 53(2), 232-245..
436

437   **List of Tables**

438

439   Table 1. Chemical composition of the synthetic water.

440   **List of Figures**

441

460

461

462   Table 1. Chemical composition of the synthetic water.

Compound	NaHCO$_3$	Na$_2$SO$_4$	NaCl	KCl	CaCl$_2$.2H$_2$O	MgCl$_2$.6H$_2$O	SrCl$_2$.6H$_2$O
Mass (g) per Litter of solution	0.28	2.216	0.615	0.075	1.082	1.356	0.053

463

464

465

466

467
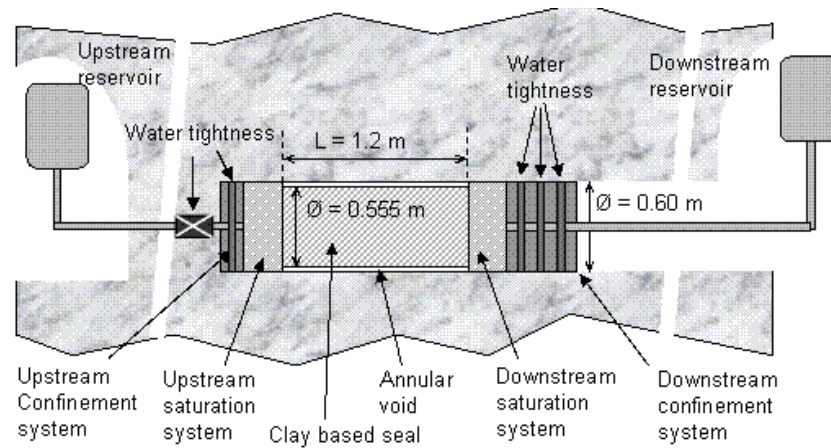
468
469

470   Figure 1. Layout of the SEALEX in-situ experiment (after Barnichon and Deleruyelle, 2009).
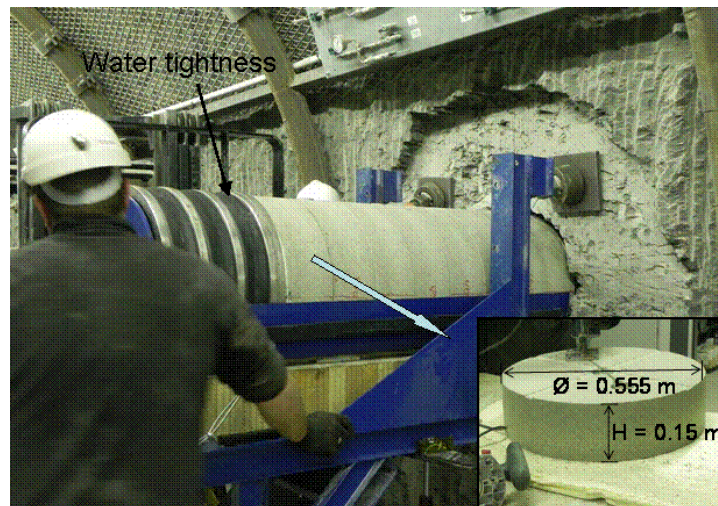
471

472   Figure 2. Geometry of the clay plug and the pre-compacted blocks.

473

474
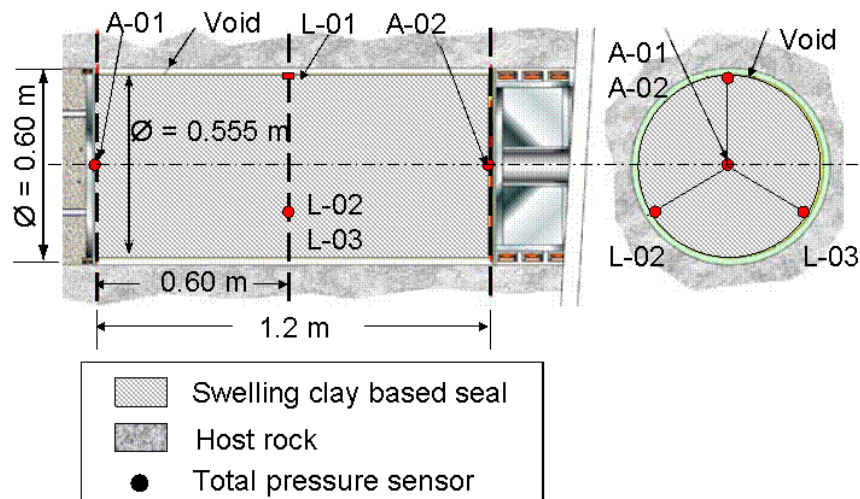
(a) Distribution of the total pressure sensors
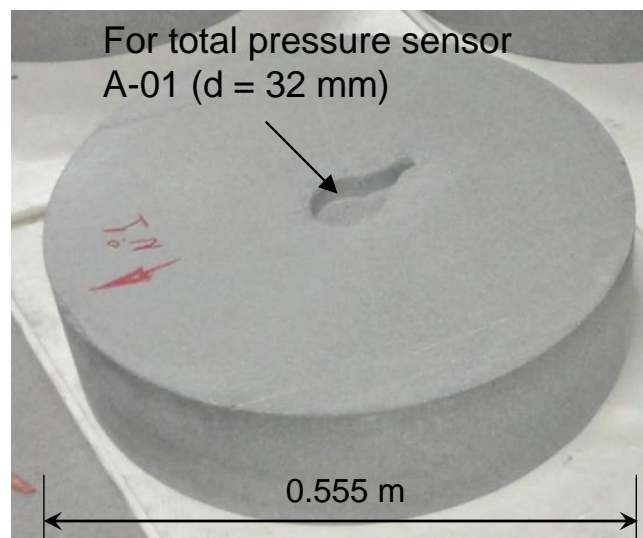
(b) Hole machined for installation of wireless sensor

Figure 3. Distribution and installation of the total pressure sensors.

481
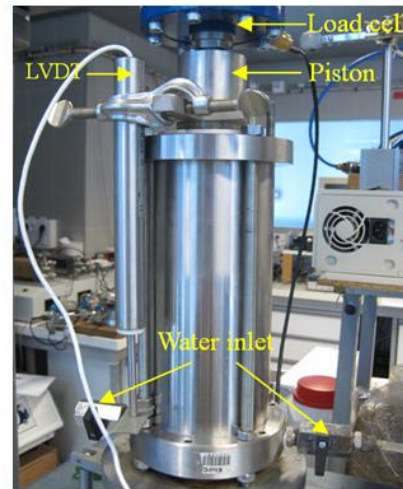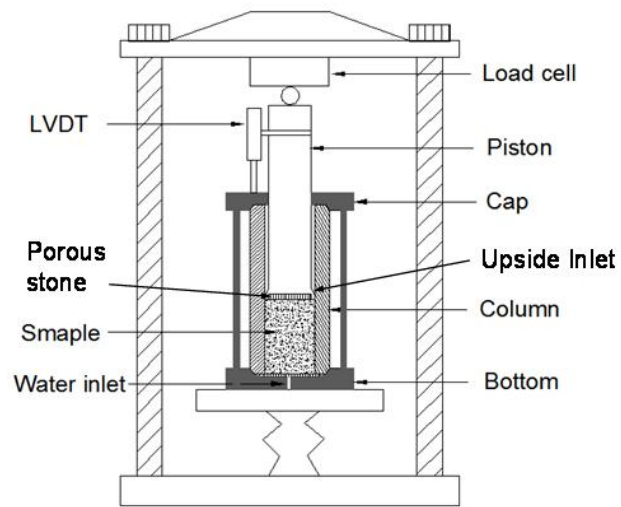
482   Figure 4. Experimental devices.

483

484   (a)   (b)
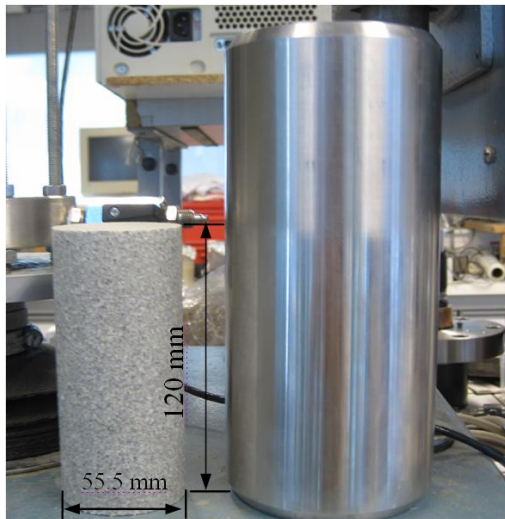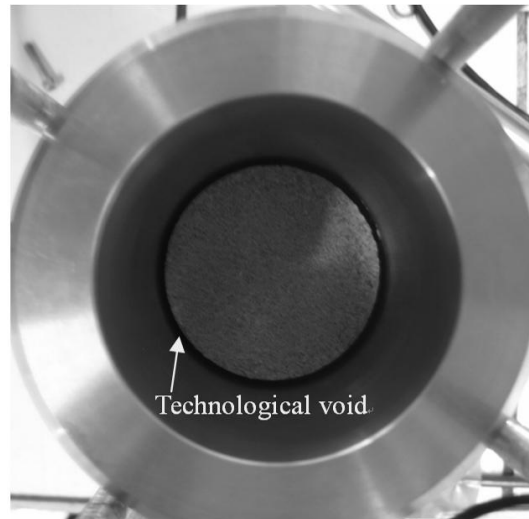
485   Figure 5. Sample preparation.

486
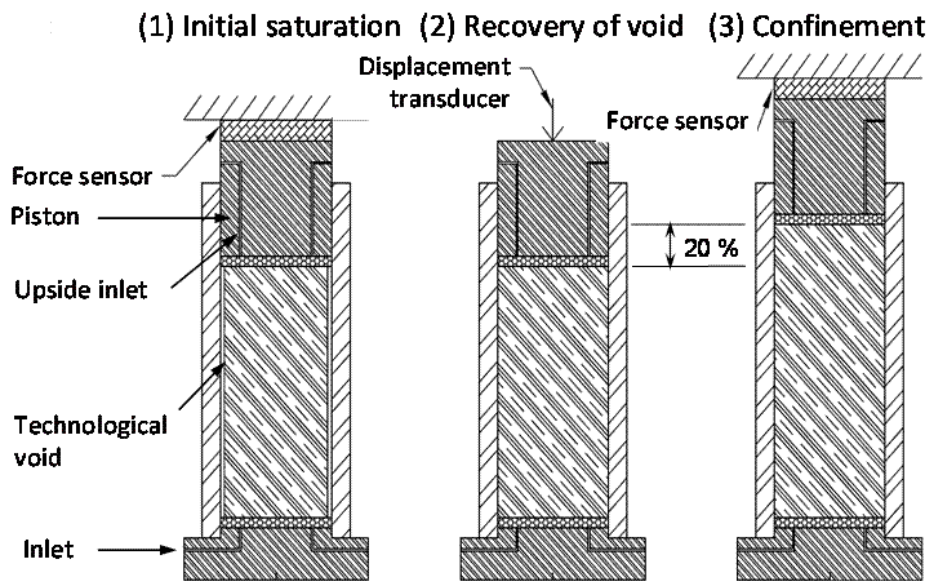
Figure 6. A schematic description of the three stages of the small-scale test.

489

490

491
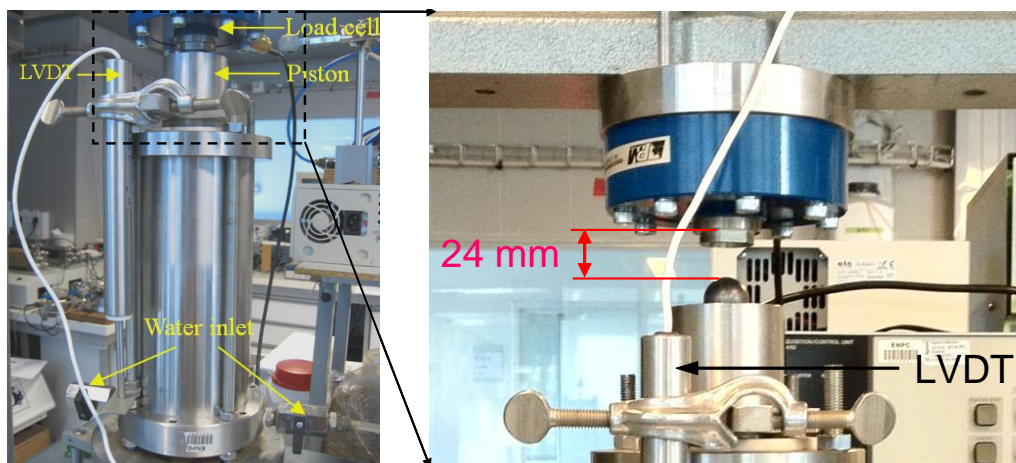
Figure 7. Lifting of load cell for free swell.

492

493
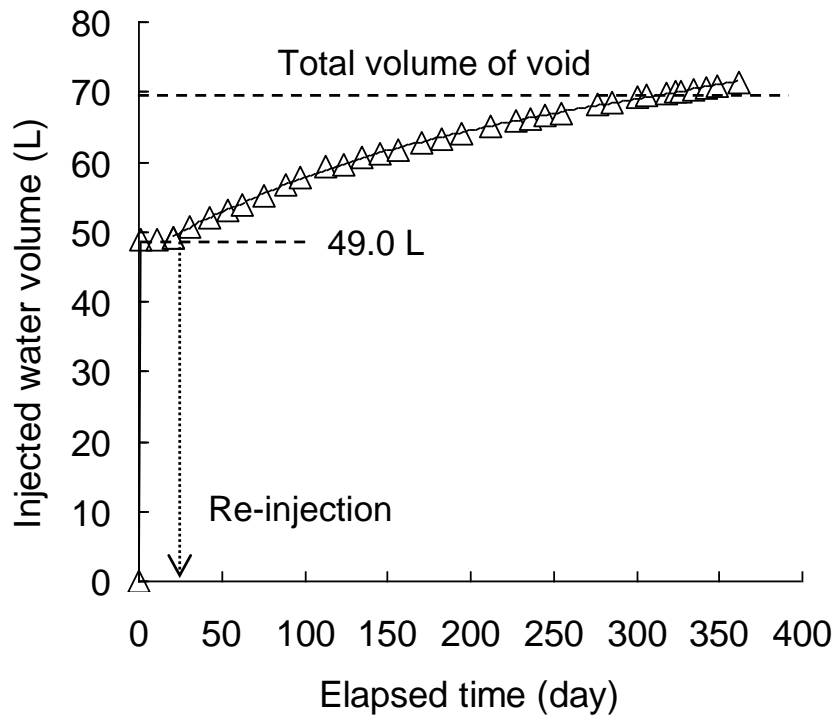
Figure 8. Injected water volume versus time.

495
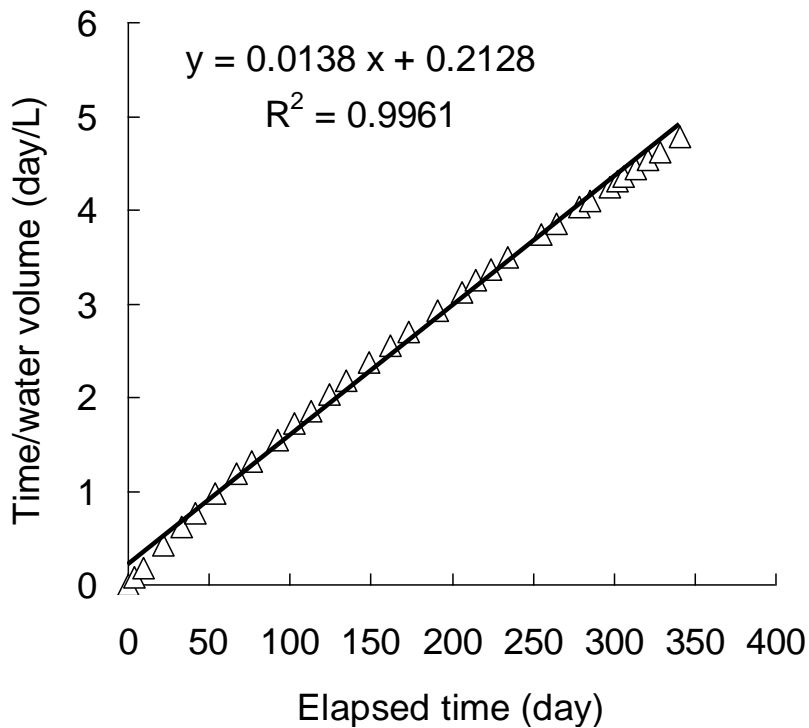
Figure 9. Time/water volume versus elapsed time after water rejection.

497
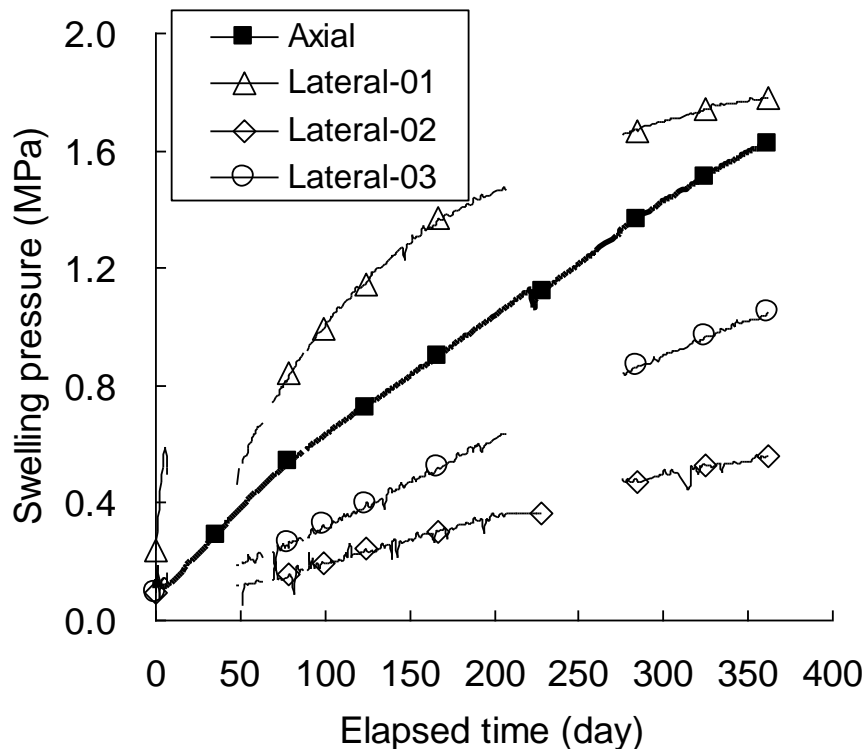
Figure 10. Evolution of swelling pressure.

499
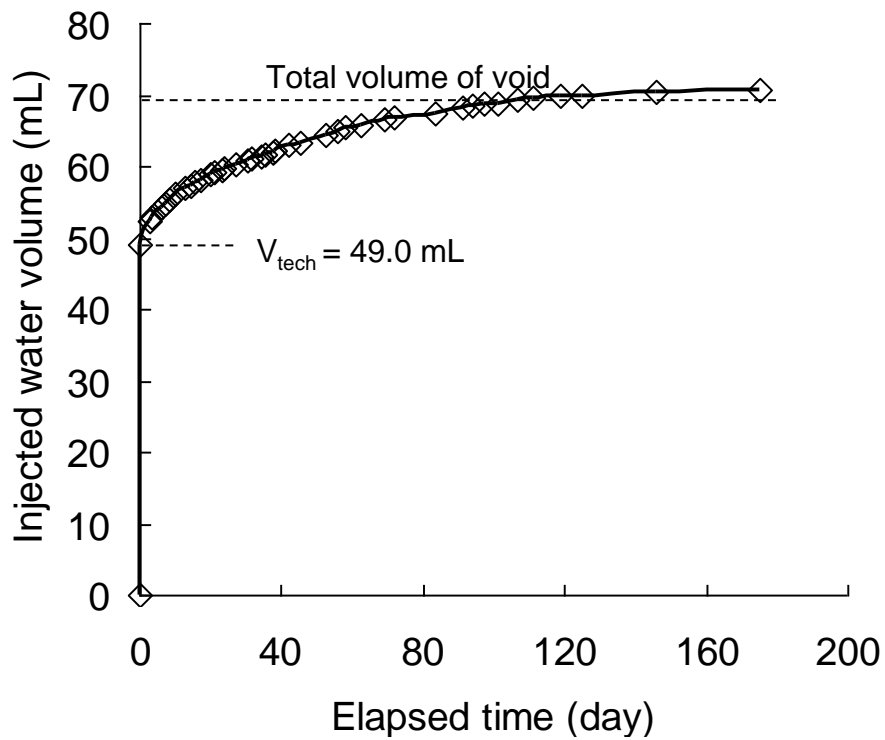
Figure 11. Water volume injected into the specimen.

28

501
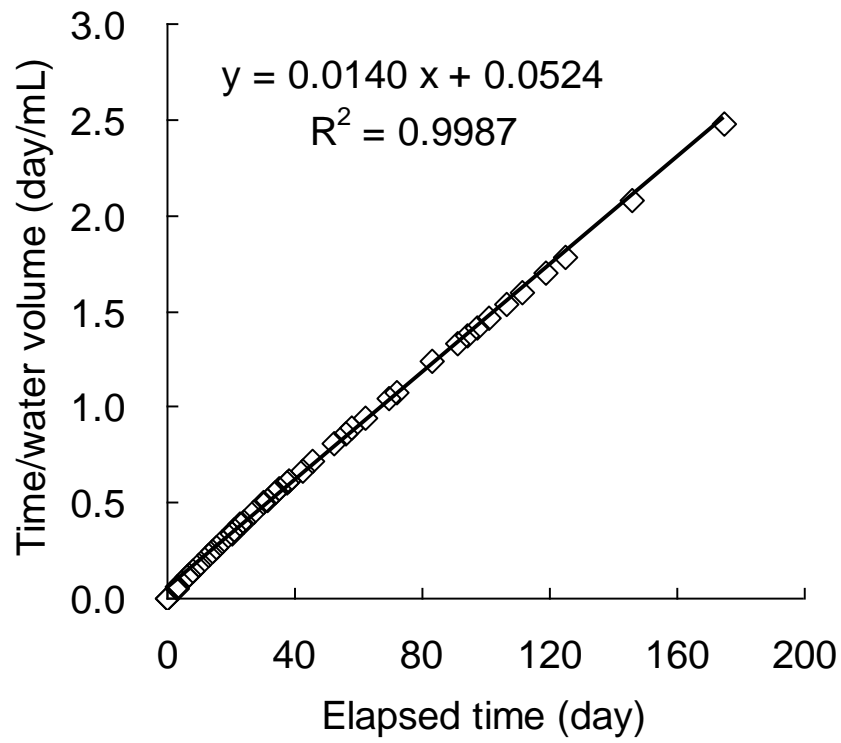
Figure 12. Time/water volume versus elapsed time.

503
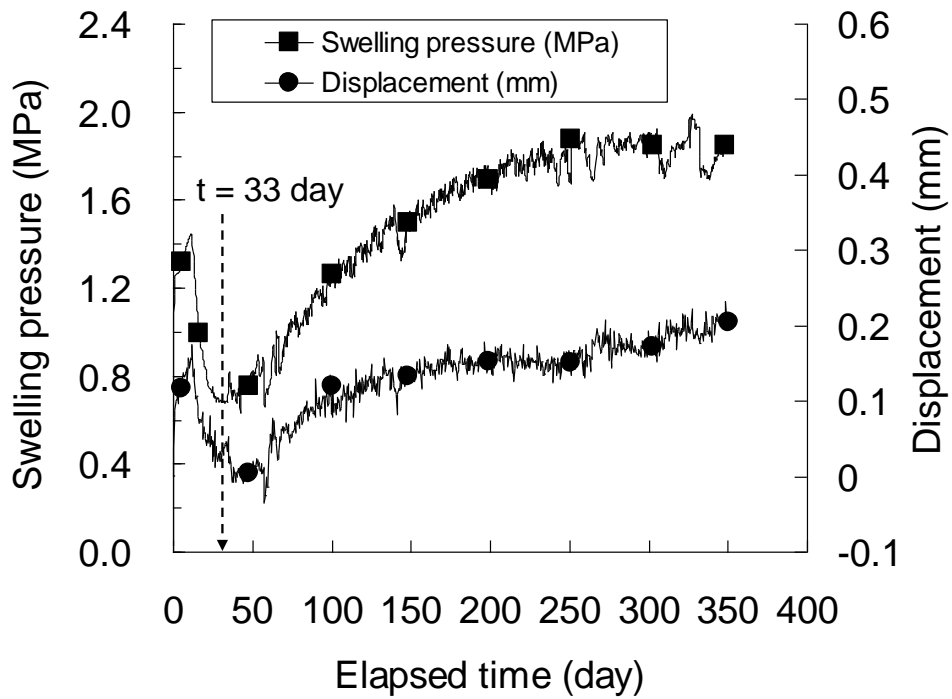
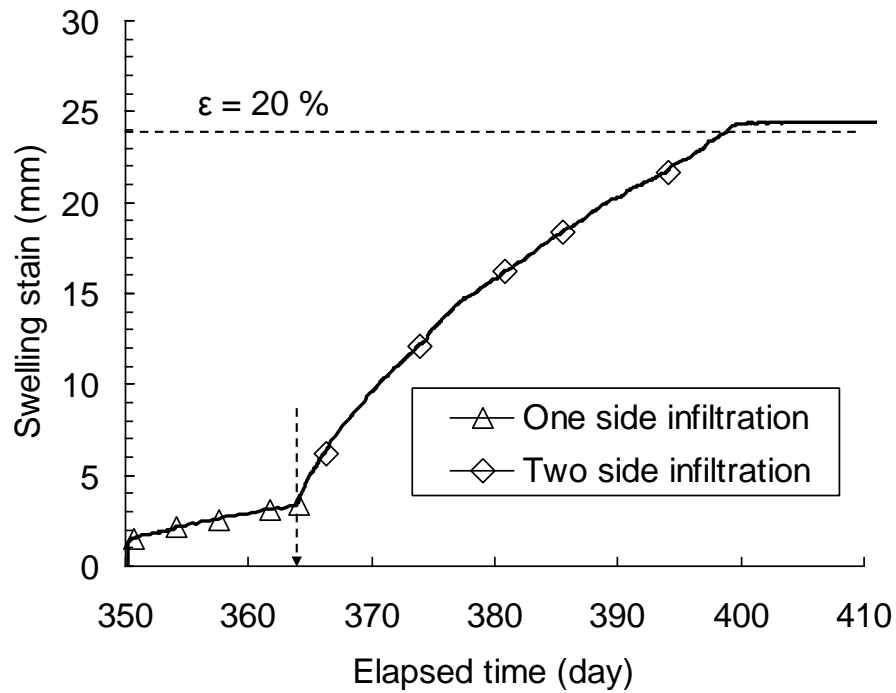Figure 13. Evolution of axial swelling pressure and displacement in the first stage.

505
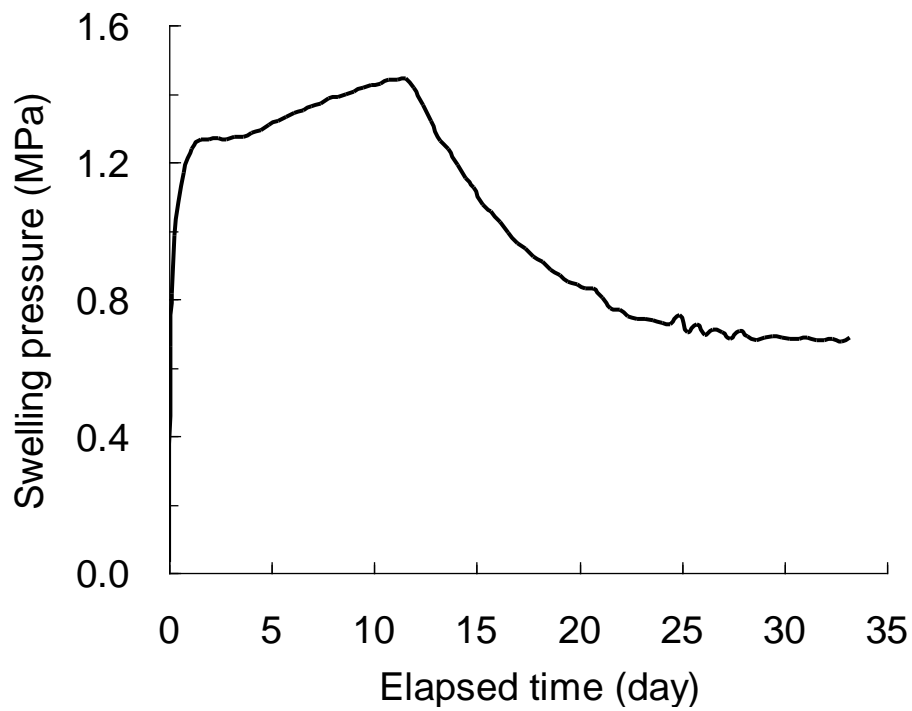
506   Figure 14. Evolution of swelling pressure during the first 33 days.

507
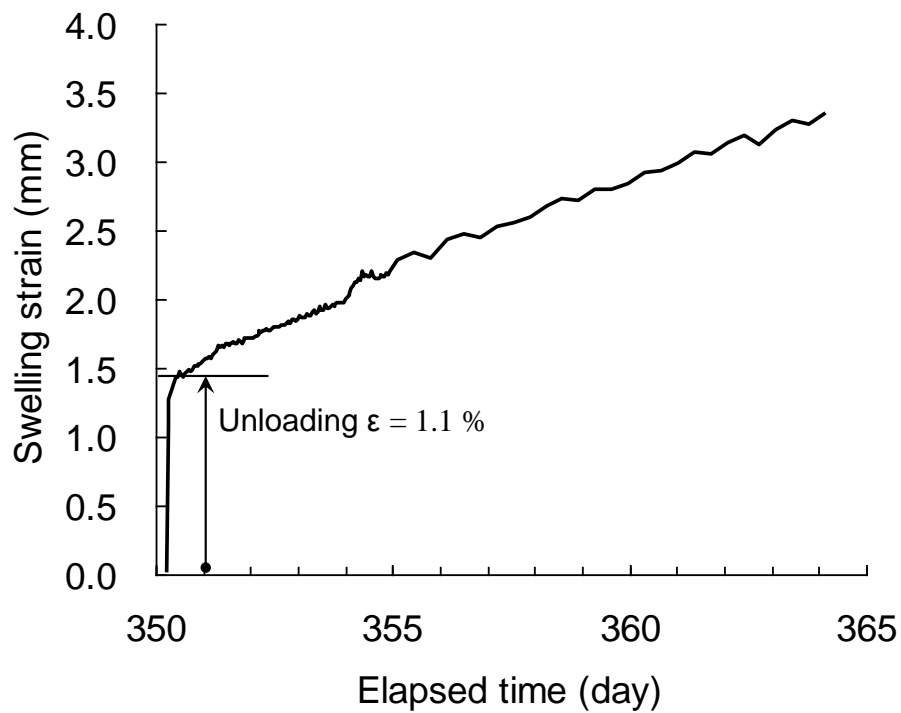
508   (a) Evolution of axial swelling strain during the first 15 days after unloading.

509

510   (b) Evolution of axial swelling strain

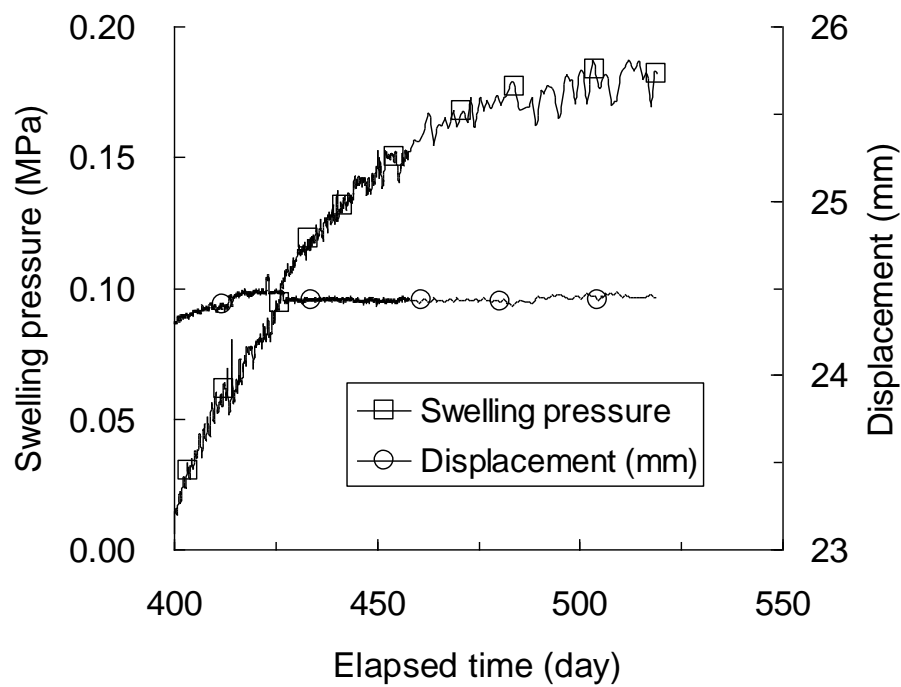511   Figure 15. Evolution of axial swelling strain during Stage 2.

512

513   Figure 16. Evolution of axial swelling pressure during Stage 3.
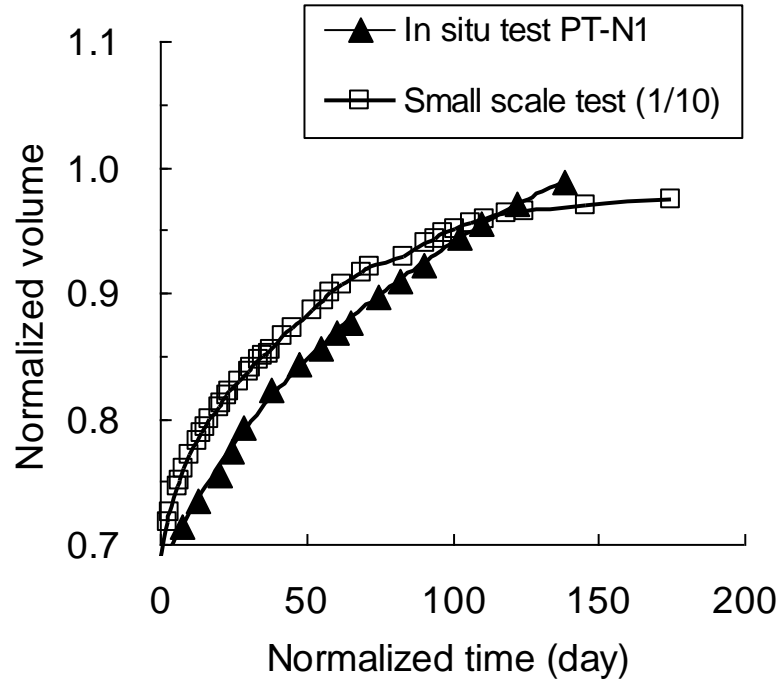
514

515   Figure 17. Normalized water volume versus normalized time.
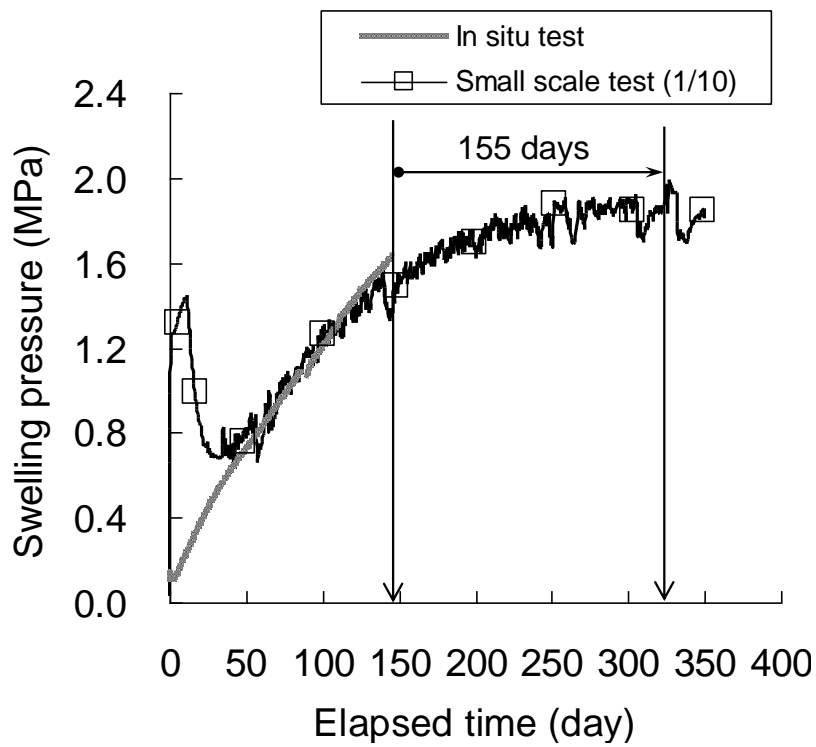

516

517   Figure 18. Swelling pressure versus normalized time.

518